



Supplementary Materials for

Unraveling the Mechanism of Protein Disaggregation Through a ClpB-DnaK Interaction

Rina Rosenzweig,^{*} Shoeib Moradi, Arash Zarrine-Afsar, John R. Glover, Lewis E. Kay^{*}

^{*}To whom correspondence should be addressed. E-mail: rina.rosenzweig@utoronto.ca (R.R.),
kay@pound.med.utoronto.ca (L.E.K.)

Published 7 February 2013 on *Science* Express
DOI: 10.1126/science.1233066

This PDF file includes:

Materials and Methods
Figs. S1 to S9
Tables S1 to S3
References (32–67)

Other Supplementary Material for this manuscript includes the following:
(available at www.sciencemag.org/cgi/content/full/science.1233066/DC1)

Coordinates for the ClpB-DnaK complex (Text and PDB format)

Correction: In the "Nucleotide release, Figure 3C" section on page 9, the value of K_d and A has been corrected and a citation to reference 25 has been added. Two additional references, 32 and 62, were also added on page 2 line 5 and page 8 line 37, respectively.

Materials and methods

Construct preparation

The DNA fragments encoding *Thermus thermophilus* ClpB (TClpB), ClpB^{NBD1-CCD} (aa 141-520) (32), ClpB^{NBD1} (aa 141-396), ClpB^{NBD2} (aa 520-845) (32), ClpB^{NTD} (aa 1-141), ClpB^{ΔNBD2} (aa 1-520) and ClpB^{ΔN} (aa 141-854) (32) were generated by PCR using TClpB in pET21c (7) as a template and subsequently cloned into a modified pET28b vector, with the thrombin cleavage site replaced by a six-histidine tag followed by a tobacco etch virus (TEV) protease cleavage site. TDnaK, TDnaJ and TGrpE constructs were synthesized by GenScript Corp (Piscataway, NJ) in fusion with an N-terminal 6xHis tag and TEV cleavage site, and sub-cloned into the NdeI and BamHI sites of pET29b (Novagen). The BAP variant of ClpB (3) was generated by replacing residues Ser712–His739 of TClpB by the P-loop region of *E. coli* ClpA (Val609-Ile635) using the restriction free cloning approach (33, 34). Mutations to ClpB, ClpB fragments and DnaK proteins were introduced using the Quikchange (Stratagene) approach and verified by DNA sequencing.

Protein expression and purification

Purification of ClpB, ClpB^{NBD1-CCD}, ClpB^{NBD1}, ClpB^{NBD2}, ClpB^{ΔNBD2}, ClpB^{ΔN} and ClpB^{NTD}

Escherichia coli BL21(DE3) codonPlus cells were transformed with modified pET28b plasmids encoding ClpB or ClpB variants. The cells were grown at 37 °C in M9 D₂O media supplemented with ¹⁵NH₄Cl or ¹⁴NH₄Cl and [²H,¹²C]-glucose as the sole nitrogen and carbon sources, respectively. Methyl labeling of the Ile-δ1-[¹³CH₃] and Val/Leu-[¹³CH₃, ¹²CD₃] variety (referred to as ILV-protein in what follows, that is U-[¹⁵N, ²H], Ileδ1-[¹³CH₃], Leu,Val-[¹³CH₃, ¹²CD₃]-labeled; note I-protein refers only to Ile-δ1-[¹³CH₃] labeling) followed the procedure of Tugarinov *et al.* (35). *E. coli* BL21(DE3)-codonPlus cells expressing unlabelled ClpB or ClpB variants were grown in Luria Bertani Broth (LB) medium. Cells were grown to OD₆₀₀ ≈ 0.8 and expression was induced by addition of 1 mM IPTG and allowed to proceed overnight at 25 °C. Following expression, bacteria were harvested and the proteins were purified on Ni-NTA resin (GE Healthcare), followed by cleavage of the purification tag using TEV protease and a HiPrep DEAE FF 16/10 column. The cleaved proteins were concentrated on an Amicon Ultra-15 30K molecular weight cutoff (MWCO) filter (Millipore) and further purified on a HiLoad 16/60 Superdex 200 pg gel filtration column (GE Healthcare), equilibrated with 50 mM Hepes, 20 mM KCl, pH 7.0, 0.03% NaN₃, with the exception of ClpB^{NBD1} that was purified on a HiLoad 16/60 Superdex 75 pg gel filtration column (GE Healthcare) equilibrated with the same buffer. ClpB and ClpB^{ΔN} eluted as single peaks at ~64 ml and ~69 ml, respectively, corresponding to their assembly into ~580 kDa and ~490 kDa hexamers. ClpB^{NBD1-CCD}, ClpB^{NBD2}, and ClpB^{ΔNBD2} eluted according to their monomeric molecular weights at ~84 ml, ~88 ml and ~78 ml, respectively. ClpB^{NBD1} eluted from HiLoad 16/60 Superdex 75 at ~69 ml, corresponding to its monomeric molecular weight of 30 kDa. The purity was confirmed by SDS-PAGE and ESI-MS.

In case of the ClpB NTD fragment (aa 1-141), *E. coli* BL21(DE3) cells expressing ClpB¹⁻¹⁴¹ in a pProEx (Invitrogen) vector were grown at 37 °C in M9 H₂O media supplemented with ¹⁵NH₄Cl as the sole nitrogen source and [¹H, ¹³C]-glucose as the carbon source. The cells were grown to OD₆₀₀ ≈ 0.6 and expression was induced by addition of 1 mM IPTG and allowed to proceed overnight at 25°C. Following expression the bacteria were harvested and the protein purified on Ni-NTA resin (GE Healthcare), followed by cleavage of the purification tag using TEV protease. The uncleaved protein and the TEV protease (with His-tag) were removed by a second purification on a Ni-NTA column. The cleaved protein was concentrated on an Amicon Ultra-15 10K molecular weight cutoff (MWCO) filter (Millipore) and further purified on a HiLoad 16/60 Superdex 75 pg gel filtration column (GE Healthcare), equilibrated with 50 mM Mops, 50 mM KCl, 10 mM MgCl₂, pH 8.2, 0.03% NaN₃, 1 mM ATP where it eluted at ~78 mL. The purity was confirmed by SDS-PAGE and ESI-MS.

DnaK, DnaK^{NBD} and GrpE purifications

BL21(DE3) cells were transformed with pET29b plasmids encoding DnaK, DnaK^{NBD} and GrpE. The cells were grown at 37 °C in M9 D₂O media supplemented with ¹⁵NH₄Cl or ¹⁴NH₄Cl as the sole nitrogen source and [²H, ¹²C]-glucose or [²H, ¹³C]-glucose as the carbon source. ILV methyl labeling followed the procedure of Tugarinov et al. (35). *E. coli* BL21(DE3)-codon plus cells expressing unlabelled DnaK, DnaK^{NBD}, or GrpE proteins were grown in LB media. Cells were grown to OD₆₀₀ ≈ 0.8 and expression was induced by addition of 1 mM IPTG and allowed to proceed overnight at 25 °C. Addition of guanidine-HCl (6 M) with heating (80 °C) was required to denature DnaK, DnaK^{NBD}, or GrpE to allow re-protonation of all amide groups in the perdeuterated protein and/or complete removal of the bound nucleotide or *E. coli* contaminants. The proteins were purified on Ni-NTA resin (GE Healthcare) and refolded on the column as described in (36), followed by cleavage of the purification tag using TEV protease and a HiPrep DEAE FF 16/10 column. DnaK was further purified on a HiLoad 16/60 Superdex 200 pg gel filtration column (GE Healthcare), equilibrated with 50 mM Hepes, 20 mM KCl, pH 7.0, 10 mM MgCl₂, 0.03% NaN₃. Additional purification of DnaK^{NBD} and GrpE was achieved using a HiLoad 16/60 Superdex 75 pg gel filtration column (GE Healthcare), equilibrated with 50 mM Hepes, 20 mM KCl, pH 7.0, 10 mM MgCl₂, 0.03% NaN₃. The purity of all proteins was confirmed by SDS-PAGE and ESI-MS.

DnaJ (37), GrpE (38), GroEL (39), GroES (39), firefly luciferase (40), ClpP (41), GFP (42), and RCMLa (40) were prepared as described.

In what follows all protein concentrations refer to monomeric ClpB^{NBD1-CCD}, ClpB^{ΔNBD2}, ClpB^{NBD2}, ClpB^{NTD}, GFP, firefly luciferase, and DnaK, dimeric DnaJ and GrpE, hexameric ClpB, heptameric ClpP and tetradecameric GroEL/ES.

NMR spectroscopy

Data analysis

All spectra were processed using the program NMRPipe (43) and chemical shift assignments were performed with the program Sparky (44).

Assignments of ClpB^{NTD} backbone and methyl side chains

NMR samples (2 mM) of purified ClpB^{NTD} (residues 1-141) were prepared in 20 mM Mops, 25 mM KCl pH 7.0, containing 7% D₂O and 0.02% (w/v) NaN₃. Data for assignments were acquired at 25 °C, 11.7T, including HNCO, HNCACO, HNCACB, and CBCA(CO)NH experiments (45, 46). A total of 133 out of 136 non-proline backbone residues were successfully assigned. These were followed by side chain assignments for 36 out of 38 methyl containing residues using (H)C(CO)NH-TOCSY, H(CCO)NH-TOCSY (47, 48), and HCCH-TOCSY experiments (49).

Chemical shift assignments for ClpB coil-coil domain methyl groups

Methyl-TROSY spectra (9) were recorded on per-deuterated protein samples dissolved in 100% D₂O, 25 mM Hepes, pH 8.5, 25 mM KCl, 10 mM MgCl₂, 1 mM EDTA, 5 mM ADP, 0.03% NaN₃, 55 °C, 18.8T. In order to assign the methyl residues in ClpB^{NBD1-CCD} a total of 15 Ile to Leu or Leu/Val to Ile point mutations were made (V473I, L492I, V504I, L486A, L479I, L460I, L420I, I415L, I459, I435, I446, I477, I362L, V511A, and I403L). A combined analysis of methyl-TROSY spectra of mutant and wild-type (wt) proteins and a 3D NOESY data set (mixing time of 200 ms; ¹³C chemical shifts of both proximal methyls are recorded (50)) allowed unambiguous assignment of 50 out of 51 methyl peaks. The observed pattern of intra- and intermolecular NOEs was carefully compared with the network of short-range methyl-methyl distances in the crystal structure (1QVR (30)).

Assignment of DnaK^{NBD} methyl residues

NMR samples (3 mM) of purified DnaK^{NBD} were prepared in 20 mM Hepes buffer at pH 6.8, 25 mM KCl, 5 mM MgCl₂, 5mM ADP·Pi containing 7% D₂O and 0.02% (w/v) NaN₃. NMR data were acquired at 55 °C, 18.8T. Backbone assignments were transferred from the BMRB (Biological Magnetic Resonance Data Bank; entry 6229) and verified using TROSY versions (51) of the following 3D experiments: HNCO, HNCACO, HNCA, HN(CO)CA (52, 53). Side-chain ¹³C and ¹H chemical shifts were obtained via (H)C(CO)NH-TOCSY, H(CCO)NH-TOCSY, and HN-methyl NOE experiments (54). Additionally, 7 mutations were made to assign methyl residues with no corresponding TOCSY peaks and the resulting assignments of 168/185 methyls were verified using methyl-methyl restraints from NOE spectra recorded on ILV-labeled DnaK^{NBD} dissolved in D₂O. Stereospecific assignment of Val and Leu methyl groups was achieved by the method of Neri *et al* (55).

NMR chemical shift perturbations

To monitor the ClpB-DnaK interaction, NMR titrations were carried out using 2D ¹⁵N-¹H TROSY-HSQC or ¹³C-¹H HMQC experiments, 18.8T. First, an ILVM-ClpB^{ΔNBD2} sample (300 μM concentration) was titrated with increasing amounts of U-[²H,¹⁴N] DnaK or DnaK^{NBD} (25, 50, 100, 150, 200, 300, 400, 500, and 600 μM), 51.5 °C. Additional binding studies were performed with a U-[¹⁵N,²H] DnaK^{NBD} sample at a concentration of 400 μM that was titrated with fully deuterated unlabeled ClpB^{ΔNBD2} (concentrations of 10, 25, 50, 100, 200, 300, 400, 500, and 600 μM), 51.5 °C. An ILVM-DnaK sample (300 μM) was also titrated with U-[²H,¹⁴N,¹²C] hexameric ClpB or ClpB^{ΔNBD2} (1, 2, 5, 10, 20, 30, 60, 90, 150, 225, 300, 450, and 600 μM hexamer

concentration), 51.5 °C. Chemical shift changes that were greater than one standard deviation from the mean were considered significant. Chemical shift perturbations (CSPs, see Figure 1) were calculated from the relations,

$$\Delta\delta = \sqrt{\left(\frac{\Delta\delta_H}{\alpha}\right)^2 + \left(\frac{\Delta\delta_C}{\beta}\right)^2} \quad [1a]$$

$$\Delta\delta = \sqrt{\Delta\delta_H^2 + \left(\frac{\Delta\delta_N}{5}\right)^2} \quad [1b]$$

in the case of perturbations to methyl (1a) or amide (1b) peak positions. In Eq. [1] $\Delta\delta$ is the shift change between apo and fully saturated forms of the protein, α (β) is one standard deviation of the methyl ^1H (^{13}C) chemical shifts (separate values of α/β are used for different methyl groups), deposited in the Biological Magnetic Resonance Data Bank.

K_d values were calculated by a nonlinear least-squares analysis using the equation

$$\Delta\delta' = \Delta\delta'_{MAX} \frac{[L]_T + [P]_T + K_d - \sqrt{([L]_T + [P]_T + K_d)^2 - 4[P]_T[L]_T}}{2[P]_T} \quad [2]$$

where $[P]_T$ and $[L]_T$ are the total protein (NMR labeled) and ligand (unlabeled) concentrations at each aliquot, $\Delta\delta'$ is the change in peak position with each aliquot and $\Delta\delta'_{MAX}$ is the change in shifts between apo and fully bound states of the protein, P . Binding isotherms were quantified separately for ^1H and ^{13}C chemical shifts.

In the case of binding of two partners, each with a single site of interaction, $[P]_T$ and $[L]_T$ correspond to the concentrations of protein and ligand, respectively, as described above. An example, is the binding of DnaK to ClpB $^{\Delta\text{NBD2}}$ or ClpB $^{\text{NBD1-CCD}}$, where both fragments of ClpB are monomeric and hence contain only a single DnaK binding site. The situation with wt-ClpB (hexamer) is potentially more complex as there are conceivably up to n=6 DnaK binding sites within each molecule, with the possibility of cooperativity between the sites (*i.e.*, non-independent binding events). A treatment of all the different binding scenarios is beyond the scope of analysis here, especially considering that titration data has been collected on a 650 kDa complex that is challenging for NMR studies. While it is difficult to distinguish between models with n=1 to 6 binding sites on ClpB on the basis of goodness of fit criteria, it is interesting to note that fitting the data with n=1 yields K_d values that are in excellent agreement with those obtained for the fragments, where binding is of necessity 1:1. This is consistent with, but does not prove, a binding stoichiometry of one molecule of DnaK per ClpB hexamer. By contrast, assuming n=6 increases the extracted K_d by close to a factor of 50 (in the limit of independent binding events).

R_1 and $R_{1\rho}$ relaxation measurements

NMR samples (1.5 mM) of a complex of U- $[^2\text{H}, ^{15}\text{N}]$ -DnaK $^{\text{NBD}}$ U- $[^2\text{H}, ^{14}\text{N}]$ -ClpB $^{\text{NBD1-CCD}}$ were prepared in 20 mM Hepes buffer at pH 6.8, 25 mM KCl, 5 mM MgCl_2 , 5mM ADP·Pi containing 7% D_2O and 0.02% (w/v) NaN_3 . NMR experiments

for the measurement of ^{15}N R_1 and $R_{1\rho}$ values, 51.5 °C 18.8T made use of TROSY versions of pulse sequences described elsewhere (46). The ^{15}N R_1 data were acquired using relaxation delays of 10, 60, 170, 360, 880, and 1250 ms while ^{15}N $R_{1\rho}$ rates were quantified using relaxation delays of 2, 6, 10, 14, 18, and 25 ms. R_2 values were calculated from R_1 and $R_{1\rho}$ rates according to the equation $R_{1\rho} = R_1 \cos^2\theta + R_2 \sin^2\theta$, where $\theta = \arctan(\omega_{\text{SL}}/\Delta\omega)$, $\Delta\omega$ is the resonance offset from the spin-lock carrier and ω_{SL} is the spin-lock field strength in the ^{15}N $R_{1\rho}$ experiments (1.84 kHz). Values of relaxation rates were obtained by non-linear least-squares fitting of the experimental data to a mono-exponential decay function, $A \exp(-R_i T)$, $R_i = \{R_1, R_{1\rho}\}$.

R_2/R_1 ratios for structured regions within the protein were used to estimate an approximate overall correlation time of the DnaK^{NBD}-ClpB^{NBD1-CCD} complex using the program r2r1diffusion (56). A value of $\tau_{c, \text{eff}} = 32 \pm 2$ ns was obtained, that is in good agreement with $\tau_{c, \text{eff}} = 28$ ns estimated on the basis of the program HYDRONMR (28 ns) (57).

A structural model for the ClpB-DnaK^{NBD} complex

MTSL spin labeling

Labeling of ClpB^{NBD1-CCD} with spin-label was achieved by introducing a single Cys mutant at the desired position (A77, E222, L479, and A502). Purified Cys mutants, stored with 5 mM DTT, were buffered exchanged into 1 mL of degassed 25 mM Hepes, pH 8.5, 25 mM KCl, 10 mM MgCl₂, 5 mM ADP, 1 mM EDTA, 0.02% NaN₃ buffer. MTSL (*S*-(2,2,5,5-tetramethyl-2,5-dihydro-1H-pyrrol-3-yl)methyl methanesulfonylthioate) spin label (Toronto Research Chemicals) was subsequently added in 3-fold molar excess and the reaction allowed to occur for 1 h at room temperature. The reaction was terminated by exchange into NMR buffer. All samples were submitted for mass confirmation (mass spectrometry) to ensure proper labeling. After NMR datasets were recorded on the oxidized samples (see below), reduced samples were generated through the addition of excess DTT, followed by buffer exchange.

Measurement of PRE values

MTSL spin labels were placed at positions 77, 222, 479, and 502 in ClpB^{NBD1-CCD} or ClpB^{ΔNBD2} (position 77) and methyl ^1H relaxation rates were recorded in the oxidized (R_2^{ox}) and reduced (R_2^{red}) states to obtain the PRE rate, $\Gamma_2^{\text{CH3}} = R_2^{\text{ox}} - R_2^{\text{red}}$. Relaxation rates were measured using a ^{13}C - ^1H HMQC type pulse scheme that selects for only the slowly relaxing ^1H magnetization components, with a variable delay included during which transverse ^1H magnetization is allowed to relax (58). This delay was set to 1, 5, 7, 10, 12, 15, 20, 30, 40, 50 ms. Measured peak intensities in two-dimensional correlation maps were fitted to extract R_2 , with errors estimated from the covariance matrix method (59). Correlations disappeared for some residues in the oxidized state; in these cases a lower bound for R_2^{ox} was estimated from the relation

$$\frac{I_{\text{ox}}}{I_{\text{red}}} = \frac{\exp(-2R_2^{\text{ox}} \tau)}{\exp(-2R_2^{\text{red}} \tau)} \cdot \left(\frac{R_2^{\text{red}}}{R_2^{\text{ox}}} \right)^2 \quad [3]$$

where I_{red} is the intensity of the correlation in the ^{13}C - ^1H spectrum recorded of the protein with the spin label in the reduced state while I_{ox} is set to 3 times the noise floor. Only contributions to relaxation of the methyl ^1H probe (*i.e.*, not the methyl ^{13}C) are considered. The value τ is the time for transfer of magnetization between ^1H and ^{13}C spins and is set to 3.5 ms. No significant changes in R_2 rates were obtained from back-to-back measurements (differences were within experimental errors) and mass-spectrometric analysis showed that samples with the MTSL spin-label remained attached to the protein after each experiment. Site-specific methyl ^1H Γ_2 rates were converted to distances from the proton in question to the paramagnetic centre using the formula (20) :

$$r = \left[\frac{\beta}{\Gamma_2} \left(4\tau_c + \frac{3\tau_c}{1 + \omega_H^2 \tau_c^2} \right) \right]^{1/6} \quad [4]$$

where $\beta = 1.23 \cdot 10^{-44} \text{ m}^6 \text{ s}^{-2}$, $\omega_H = 2\pi 800 \cdot 10^6 \text{ rad s}^{-1}$ and τ_c is set to 28 ns for the DnaK^{NBD}-ClpB^{NBD1-CCD} complex. We have not attempted to take into account the fact that the complex is asymmetric and well approximated by a prolate ellipsoid ($D_{par} / D_{perp} \sim 2.3$) because (i) the 1/6 power in Eq. [4] greatly attenuates the distance dependence on tumbling time (maximum errors of less than 10% are calculated by using an isotropic tumbling model), (ii) both the MTSL spin label and the methyl group probes used are dynamic so that the distance is not fixed and (iii) the model for DnaK^{NBD} used in structure calculations is based on homology from X-ray structures of DnaK chaperones generated using I-TASSER software (<http://zhanglab.ccmb.med.umich.edu/I-TASSER/>), and not from *Thermus thermophilus* (the version used in our study here) for which a high resolution structure is not available.

Molecular docking

A model for the ClpB-DnaK^{NBD} complex was obtained using the molecular docking program HADDOCK2.1 (22), based on CSPs for ClpB^{ΔNBD2} and DnaK^{NBD}, and long-range distance restraints obtained through PREs. Starting structures included the previously published structure for a monomer of ClpB (PDB entry 1QVR (30)) and a homology model for TDnaK^{NBD} generated using I-TASSER software (<http://zhanglab.ccmb.med.umich.edu/I-TASSER/>). Active and passive residues were selected based on the strategy outlined in reference (22). Active residues for ClpB and DnaK were those for which chemical shift changes > 0.2 ppm were observed upon binding and with high surface accessibilities (>40% backbone and/or side chain surface accessibility). Residues with high surface accessibility adjacent to active residues were chosen as passive residues. Solvent accessibility was calculated using the program NACCESS (60). All ambiguous interaction restraints, AIR (22), were defined with a maximum effective distance of 2 Å. The linker between the N-terminal domain and nucleotide binding domain 1 of ClpB was defined as being “fully flexible”, because this region has high conformational flexibility in the free form (30), see table S2.

Paramagnetic spin-label distance restraints were provided as input data to HADDOCK, along with the ambiguous restraints (AIR, *i.e.*, residues with CSPs), and were used in all stages of the docking calculations. Intermolecular distances between the MTSL nitroxide attached to ClpB^{NBD1-CCD} and the DnaK NBD methyl group

(nitroxide oxygen and methyl carbon distance) in question were calculated from paramagnetic relaxation enhancement (PRE) effects using a protein rotational correlation time of 28 ns, as described above. To the computed distance, upper and lower bounds of +3 Å and -6 Å, respectively, were added (*i.e.*, a distance range of between $r_o+3\text{Å}$ and $r_o-6\text{Å}$ was used, where r_o is the computed distance from PREs) although very similar structural models were obtained when a lower bound of -10Å was used (PRE derived distances are listed in table S2). For those correlations that disappeared upon addition of nitroxide label a lower bound distance of $r_o-10\text{Å}$ was used. Docking was initiated with random starting orientations of ClpB and DnaK^{NBD} separated by a minimum of 25 Å, with each molecule rotated randomly around its center of mass. Both non-bonded and electrostatic energy terms were included in the calculation. Next, four cycles of rotational minimization were performed, in which each molecule is allowed to rotate in turn, followed by two cycles of rotational and translational rigid body minimization in which each molecule and the associated solvent is treated as one rigid element. The best 1000 structures after rigid body minimization were subjected to a semi-flexible simulated annealing refinement protocol in torsion angle space whereby sidechains and loops were allowed to move, with the complex immersed in an 8 Å shell of TIP3P water molecules. Docked structures, corresponding to the 200 best solutions with the lowest intermolecular energies, were generated and clustered based on a backbone rmsd tolerance of 1.0 Å. The quality of the structural ensemble was assessed using the PROCHECK program (Laskowski et al., 1993).

Functional assays

Chaperone assisted aggregate reactivation (Disaggregation), Figures 2F, S6, S9

Recombinant firefly luciferase (0.2 µM) was incubated for 30 min at 30 °C in denaturation buffer (25 mM HEPES-KOH, pH 7.5, 50 mM KCl, 10 mM MgCl₂, 1 mM DTT, 6 M Urea). To form irreversible aggregates denatured luciferase was diluted 125 fold into ice-cold renaturation buffer (25 mM Hepes, pH 7.5, 50 mM KCl, 10 mM MgCl₂, 1 mM DTT, 0.1 mg/ml BSA, 1mM ATP, 20 mM creatine phosphate, 6 µg creatine kinase). The refolding reaction was started by addition of 3 µM wt ClpB or mutants of ClpB, 3 µM DnaK, 0.8 µM DnaJ and 0.4 µM GrpE to 2 nM luciferase aggregates. Luminescence was measured at various time points by addition of 50 µM of luciferase reagent (Promega) to 2 µl of the refolding reaction.

α -Glucosidase from *Bacillus stearothermophilus* (Sigma) was used as described previously (61, 62). Briefly, α -glucosidase (0.1 µM) was denatured for 10 min at 75 °C in the reaction buffer (25 mM HEPES-KOH, pH 7.5, 50 mM KCl, 10 mM MgCl₂, 5 mM ATP, 1 mM DTT). Chaperones were added (1.0 µM wt ClpB or mutants of ClpB, 1.0 µM DnaK, 0.4 µM DnaJ, 0.2 µM GrpE) prior to refolding at 55 °C. To measure the recovered α -glucosidase activity, *p*-nitrophenyl glucopyranoside was added to a final concentration of 2 mM. The reaction mixture was incubated at 40 °C for 20 min and the reaction terminated with 0.4 M sodium carbonate. The amount of *p*-nitrophenol released was measured by absorbance at 400 nm.

Recombinant enhanced GFP (4.5 µM) was heat denatured at 80 °C for 15 min. Reactivation was started by diluting the GFP 12-fold in reactivation buffer, containing

25 mM Hepes-KOH, pH 7.5, 50 mM KCl, 10 mM MgCl₂, 4 mM ATP, an ATP regenerating system, 0.13 μM ClpB, 0.43 μM DnaK, 0.08 μM DnaJ, 0.03 μM GrpE. Reactivation was monitored over time at 25°C using a SpectraMax M2 Microplate Reader. Excitation and emission wavelengths were 488 nm and 510 nm, respectively.

Degradation reactions, Figure 4C, S7C

All degradation reactions were carried out using 1 μM BAP, 1.5 μM ClpP, 1 μM DnaK, 0.2 μM DnaJ in the presence or absence of 0.1 μM GrpE. Substrates were used at the following concentrations: 2 μM casein, 1 μM luciferase, and 0.4 μM GFP. Substrate degradation was followed by gel electrophoresis and western blotting with anti-luciferase (Promega), anti-GFP (Abcam) or in the case of casein, gel electrophoresis followed by Coomassie-blue staining.

Refolding reaction, Figure 3D, S8B

MDH (2 μM) was heat denatured at 47 °C for 30 min in reaction buffer (25 mM HEPES-KOH, pH 7.5, 50 mM KCl, 10 mM MgCl₂, 5 mM ATP, 1 mM DTT) with 20 μM sHsp16.5. Luciferase (0.2 μM) was heat denatured in reaction buffer with 5 μM DnaK and 3 μM DnaJ at 43 °C for 15 min. Protein refolding was started by adding an equivalent volume of reaction buffer containing 5 μM DnaK and 1 μM GrpE at 30 °C. For competition assays involving NBD1, one of either ClpB^{NBD1-CCD}, ClpB^{NBD1} or ClpB^{NBD1-CCD} Y494A was added to a final concentration of 50 μM. The assays were performed in the presence of an ATP regenerating system (1 mM phosphoenolpyruvate, 20 μg/ml pyruvate kinase, 2 mM ATP). Determination of enzymatic activities followed published protocols (63).

Nucleotide release, Figure 3C

Stopped flow measurements were performed using a Timemaster fluorescence spectrometer (PTI) with a Kin-Tek SF-120 stopped-flow apparatus. The samples were in 50 mM HEPES-KOH (pH 7.5), 50 mM KCl, 5 mM MgCl₂, 1 mM EDTA, and 2 mM DTT buffer, and the temperature of the cuvette was held at 30 °C using a water bath. DnaK (0.5 μM) was incubated overnight at 55 °C with MABA-ATP (0.5 μM) to generate a DnaK-MABA-ADP complex. In a stopped flow experiment, the resulting complex was mixed with 1 mM ADP (to make the dissociation of MABA-ADP irreversible) in the absence or presence of GrpE or ClpB^{NBD1-CCD}. Nucleotide exchange was monitored as the decreasing fluorescence intensity of MABA-ADP upon dissociation from DnaK. A wavelength of 360 nm was used for excitation while emission was measured with a cut-off filter at 455 nm, as described in the literature (25). Fluorescence *vs* time profiles were fit to single exponential decay functions to extract rate constants for nucleotide exchange (k_{obs}). Values of k_{obs} as a function of TGrpE concentration were fitted to a hyperbolic function, $k_{obs} = A[TGrpE]/(K_d + [TGrpE])$ with $K_d = 2.1 \pm 1.0$ μM and a saturation value, A, of 5.5 ± 0.9 s⁻¹ for the maximal GrpE-stimulated nucleotide release. These values must be considered as only approximate due to the low concentrations of TGrpE that were used. The maximal stimulation of TGrpE-mediated nucleotide exchange is thus ~70,000-fold, compatible with previously published data, 80,000-fold (25). Kinetic rates were determined using Wolfram Mathematica8 software (64).

Gel-filtration analysis, Figure S7A

ClpB samples (100 μ L of \sim 20 mg/ml protein) in 50 mM MOPS-KOH, pH 8.5, 20 mM KCl, 10 mM MgCl₂, and 1 mM ATP were chromatographed on a Superose 6 GL 10/300 column (Amersham Pharmacia Biotech) using a flow-rate of 0.5 ml/min. Molecular size standards used were thyroglobulin (669 kDa), ferritin (443 kDa), aldolase (158 kDa), and conalbumin (75 kDa).

ClpB ATPase activity determination, Figure 4B, S7B

The ATPase activities of wt or mutant TClpB (10 μ M) were measured spectrophotometrically (65) with an ATP-regeneration system that contained 2.5 mM phosphoenolpyruvate, 0.2 mM NADH, 50 μ g/ml pyruvate kinase, 50 μ g/ml lactate dehydrogenase and 3 mM ATP at 55 °C (66). When indicated, α -Casein (0.1 mg/ml) or DnaK T199A (25 μ M), an ATP hydrolysis inactive mutant, was added to the reaction. The changes in absorbance at 340 nm were monitored in a V-650 spectrophotometer. All ATPase assays were performed in triplicate.

DnaK ATPase activity measurement, Figure S8A

Reaction mixtures (50 μ l) comprising 20 mM Tris-HCl, pH 7.5, 100 mM KCl, 5 mM DTT, 0.1 mM EDTA, 10% glycerol (v/v), 0.005% TritonX-100 (v/v), 20 mM MgCl₂, 5 μ M DnaK, 10 μ M DnaJ, 2 μ M GrpE, 10 to 100 μ M ClpB^{NBD1-CCD} and 50 μ M bovine serum albumin (BSA) with 4 mM ATP, 0.6 μ Ci of [γ -³²P] ATP were incubated for 120 min at 55°C. Reactions were transferred into 1 ml of a 1:1 (v/v) mixture of isobutanol and toluene plus 0.6 ml of 5 mM silicotungstate/1 mM H₂SO₄ and vortexed for 10 s. Next 0.16 ml of 5% ammonium molybdate (w/v) in 2 M H₂SO₄ was added and each tube was vortexed vigorously for 30 s. Organic and aqueous phases were separated by centrifugation in a table-top centrifuge at high speed (\sim 10000 rpm) for 2 min. The amount of ³²P_i in the organic phase (0.5 ml) were quantified by liquid scintillation spectrometry with 5 ml CytoScint (67).

Acrylodan labeling

The thiol reactive acrylodan (6-acryloyl-2-dimethylaminonaphthalene; Molecular Probes) was attached to DnaK to monitor substrate release, Figure 4A. Acrylodan was dissolved in dimethylformamide to a stock concentration of 100 mM (measured by absorbance at 387 nm; ϵ = 16,400 M⁻¹cm⁻¹ in ethanol). For fluorescence labeling, 1.5 mM DnaK S535C in 25 mM HEPES-KOH, 50 mM KCl, 5 mM MgCl₂, pH 7.5, was reacted with a 5-fold molar excess of acrylodan for 16 h at 4° C. Acrylodan-labeled DnaK was purified by size exclusion chromatography on a Superdex200 column (Amersham Biosciences). Incorporation of a single fluorophore per DnaK S535C molecule was confirmed by mass spectrometry.

Substrate release assay, Figure 4A

A Kin-Tek SF-120 stopped-flow apparatus was used to record changes in the fluorescence emission intensity of DnaK C535-acrylodan that accompanies release of the bound RCMLa. A 100 μ l solution of a 2 μ M acrylodan labeled DnaK C535 – RCMLa complex was injected with 100 μ l of a solution containing 10 μ M of one of

the proteins indicated in Figure 4A and 2 mM ATP, after equilibration of each solution for at least 10 min at 30° C. Substrate (RCMLa) exchange was monitored by following the decrease of donor fluorescence at 500 nm, with excitation at 380 nm. Kinetic rates were determined using Wolfram Mathematica8 (64).

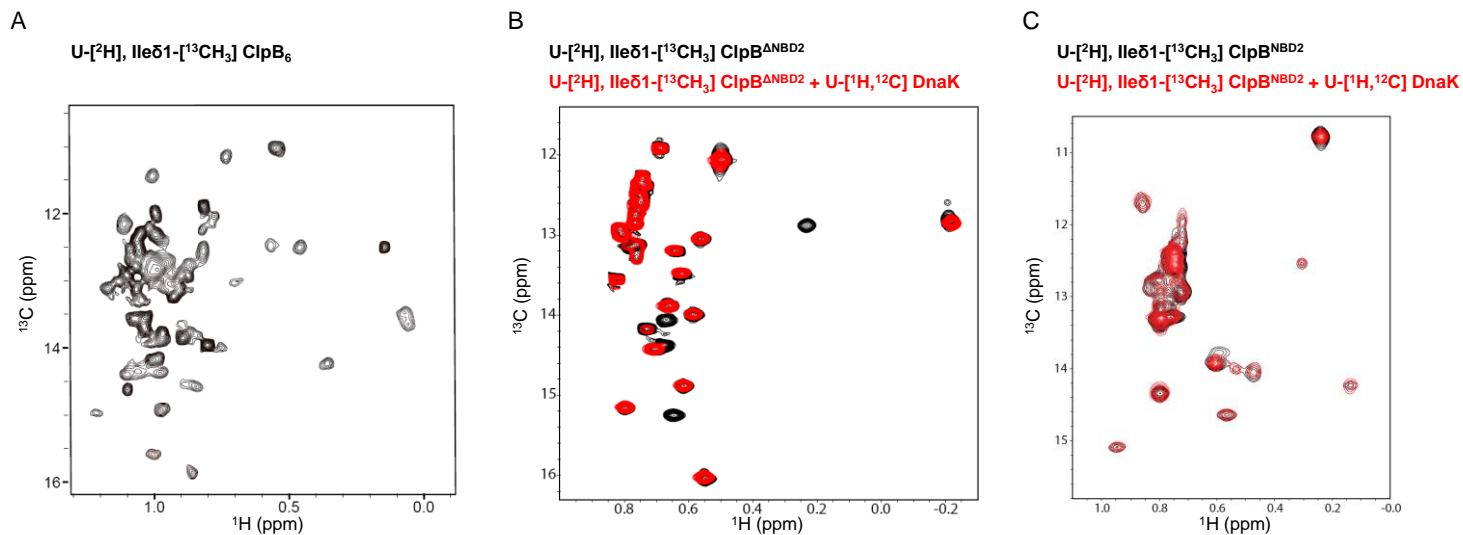


Fig. S1. DnaK interacts with the ClpB^{N-NBD1-CCD} fragment (ClpB^{ΔNBD2}) which lacks the NBD2 domain

Methyl-TROSY spectra of I-ClpB hexamer (580 kDa) (A). Methyl-TROSY spectra of I-ClpB^{ΔNBD2} (B) or I-ClpB^{NBD2} (C) titrated with 2-fold molar excess of U-[¹H, ¹²C] DnaK. Changes to spectra, including peak broadening or disappearance of resonances were only observed for the ClpB^{ΔNBD2} fragment indicating formation of a ClpB^{ΔNBD2}-DnaK complex. Data sets were recorded at 14.0T, 35°C. Note that broadening/disappearance of peaks reflects the significant relaxation of methyl magnetization from the protonated DnaK. The titrations in Figures 1B,D and 3B made use of completely deuterated binding partners.

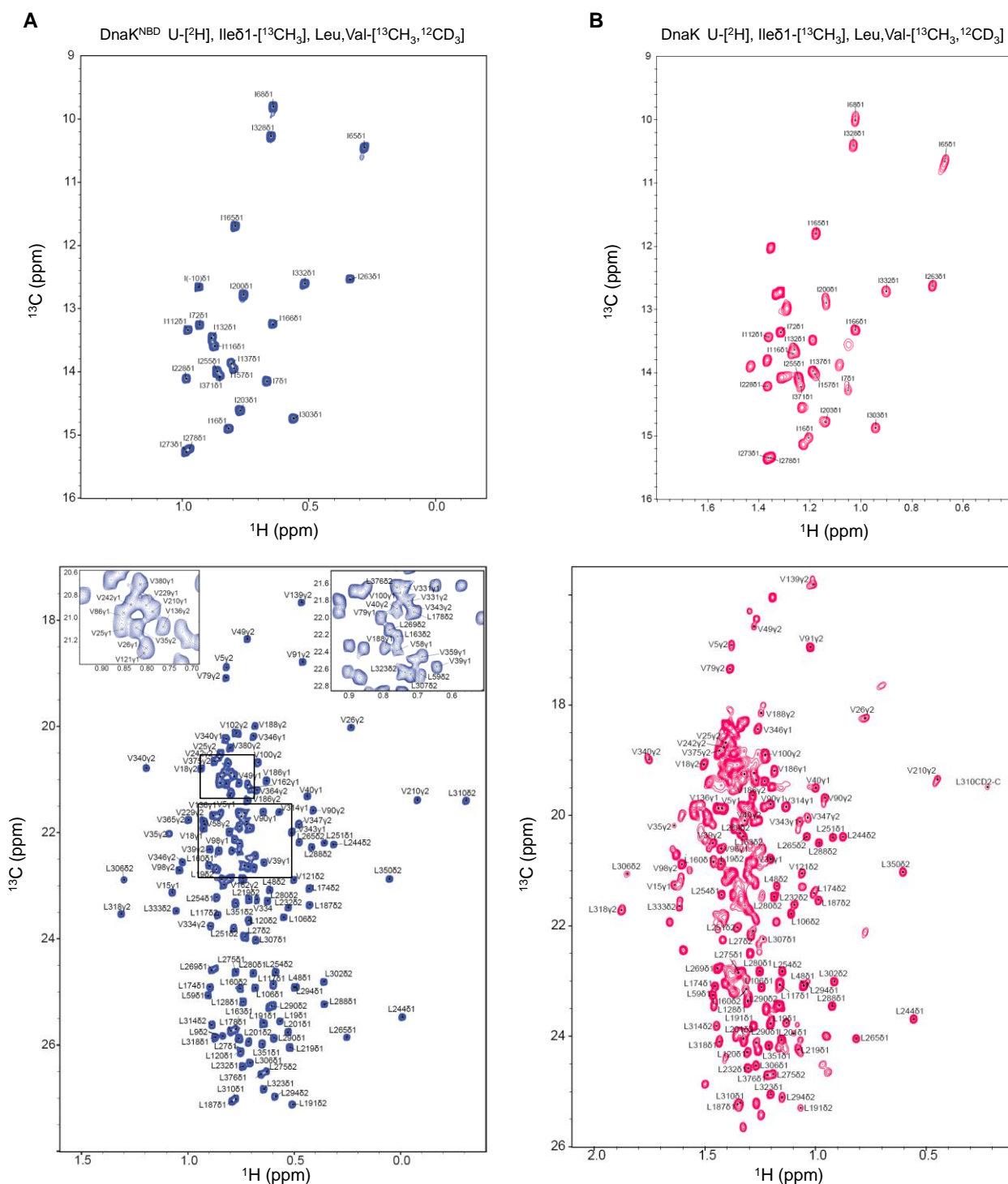


Fig. S3 Assignment of methyl residues of the DnaK nucleotide binding domain.

Methyl-TROSY spectra of ILV-DnaK^{NBD} (A) or ILV-DnaK (B) (18.8T, 51.5 °C) showing the assignments for 106 out of 107 methyl residues. (*Top*) δ1 methyl groups of Ile residues. (*Bottom*) Leu-δ1/δ2 and Val-γ1/γ2 methyl groups. Leu/Val methyl groups are labeled with their stereospecific assignments.

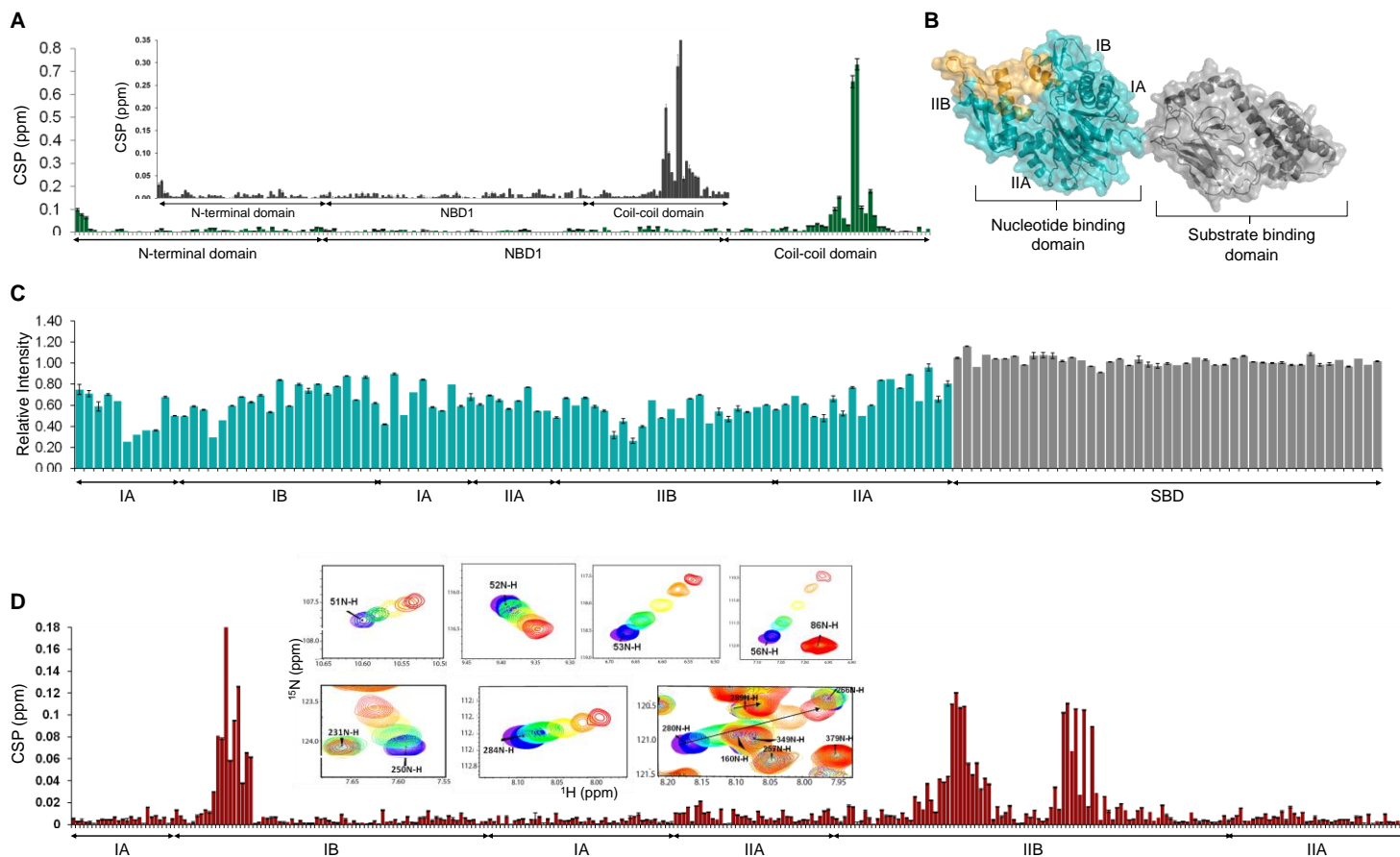


Fig. S4 ClpB interacts selectively with the nucleotide binding domain of DnaK

(A) Magnitudes of chemical shift perturbations (CSPs) for ILV-ClpB^{ΔNBD2} at the endpoint of a titration with DnaK^{NBD} (or DnaK, inset; Figure 1B) are shown as green (black) bars for each residue. ClpB^{ΔNBD2} domains are indicated along the x-axis. (B) Structural representation of DnaK chaperone, with nucleotide binding domain colored cyan and substrate binding domain colored grey. Subdomains of NBD are labeled for clarity. Region indicated in orange corresponds to the ClpB binding site. (C) Plot of HMQC peak intensities measured from a spectrum of ILV-DnaK in complex with ClpB₆, relative to those of free ILV-DnaK. SBD residues of DnaK do not show any decrease in peak intensities upon complex formation with the hexameric, 580 kDa ClpB protein. (D) Magnitudes of CSPs for ¹⁵N-DnaK^{NBD} at the endpoint of a titration with unlabeled ClpB^{NBD1-CCD} vs residue. Selected regions of ¹⁵N-¹H HSQC data sets of ¹⁵N-DnaK^{NBD} in the absence (blue) or as a function of increasing concentrations (cyan to red) of 0.2 – 2.5 molar equivalents of unlabeled ClpB^{NBD1-CCD}. Arrows indicate directions of peak movement. Residues showing CSPs > 0.05 are colored orange on panel B.

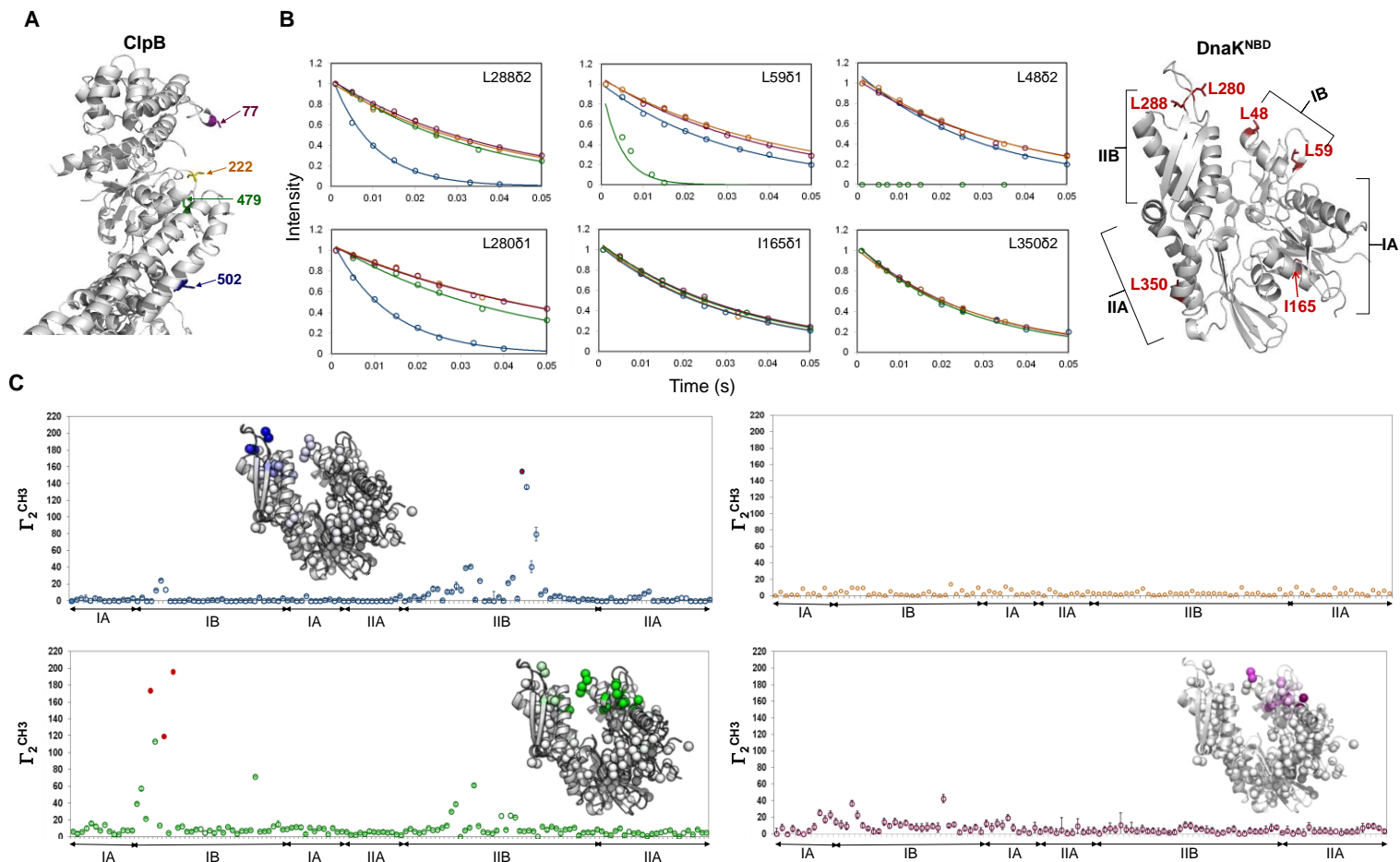


Fig. S5 Paramagnetic relaxation enhancement

(A) Paramagnetic relaxation enhancement (PRE) data from spin labels attached to one of residue 77 (purple), 222 (orange), 479 (green), or 502 (blue) for $\text{ClpB}^{\Delta\text{NBD2}}/\text{ClpB}^{\text{NBD1-CCD}}$ fragments, as monitored via methyl ^1H transverse relaxation in ILV-DnaK^{NBD}. (B) $\text{ClpB}^{\text{NBD1-CCD}}$ with MTSL attached at one of the indicated positions was complexed with ILV-DnaK^{NBD} and ^1H R_2 values were measured for oxidized and reduced samples by recording a series of two-dimensional data sets as a function of a parametrically varied transverse relaxation delay. Shown are the decay profiles for selected ^1H methyl spins on DnaK (left) and the position of these methyls within DnaK^{NBD} (right). Subdomains are mapped onto the DnaK structure. (C) PRE rate, $\Gamma_2^{\text{CH}_3} = R_2^{\text{ox}} - R_2^{\text{red}}$, where R_2^{ox} and R_2^{red} are rates recorded on oxidized and reduced samples, respectively, obtained for ILV-DnaK^{NBD} in complex with $\text{ClpB}^{\text{NBD1-CCD}}$ with the MTSL spin label positioned at 479 (green), 502 (blue), 77 (purple), or 222 (orange). Red filled circles indicate residues where cross-peaks in HMQC spectra are broadened beyond the limits of detection. Sub-domain boundaries for DnaK NBD are indicated underneath each plot. (insets) Cartoon representations of DnaK NBD with methyl residues shown as balls and color scaled according to $\Gamma_2^{\text{CH}_3}$.

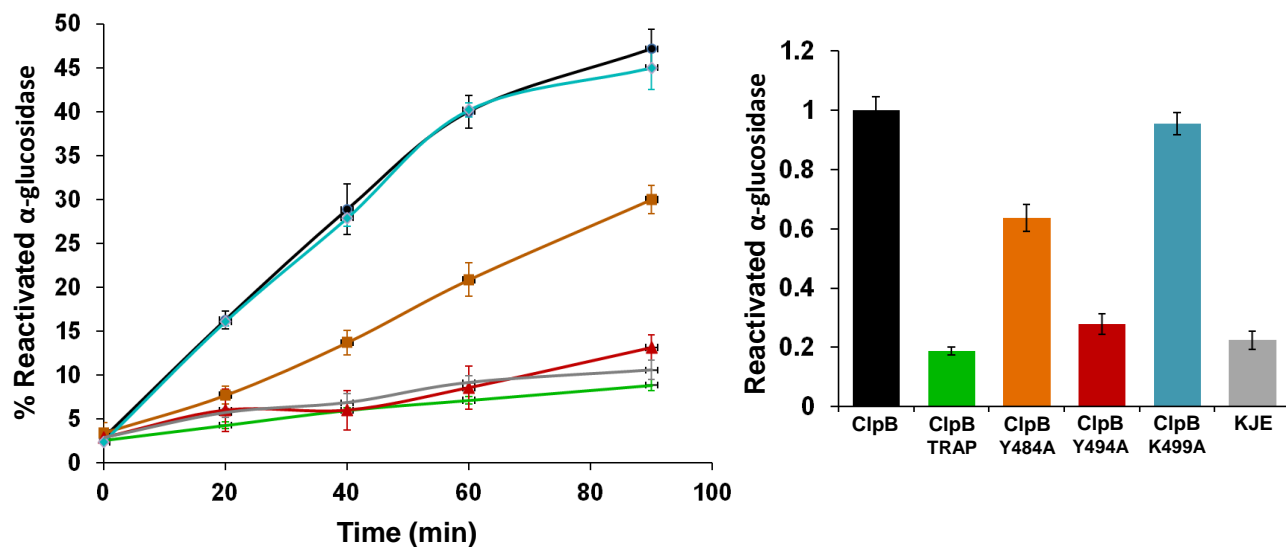


Fig. S6 Disaggregation properties of ClpB mutants in collaboration with KJE system

The disaggregation activities of ClpB mutants were determined by following the recovery of heat denatured α -glucosidase activity in the presence of DnaK/DnaJ/GrpE chaperones and indicated ClpB variants. Activity of untreated α -glucosidase was set as 100% (left). Reactivated α -glucosidase at the end of 90 min as a fraction of wt-ClpB reactivation (right). Standard errors of three independent assays are shown. ClpB K499A mutant (cyan) showed wt activity resulting in ~50% reactivation of α -glucosidase over the course of 90 minutes. ClpB^{Y484A} (orange) activity was impaired, resulting in only 60% yield of reactivated enzyme compared to wt-ClpB (black). ClpB^{Y494A} (red), which cannot form a complex with DnaK, was incapable of enzyme reactivation.

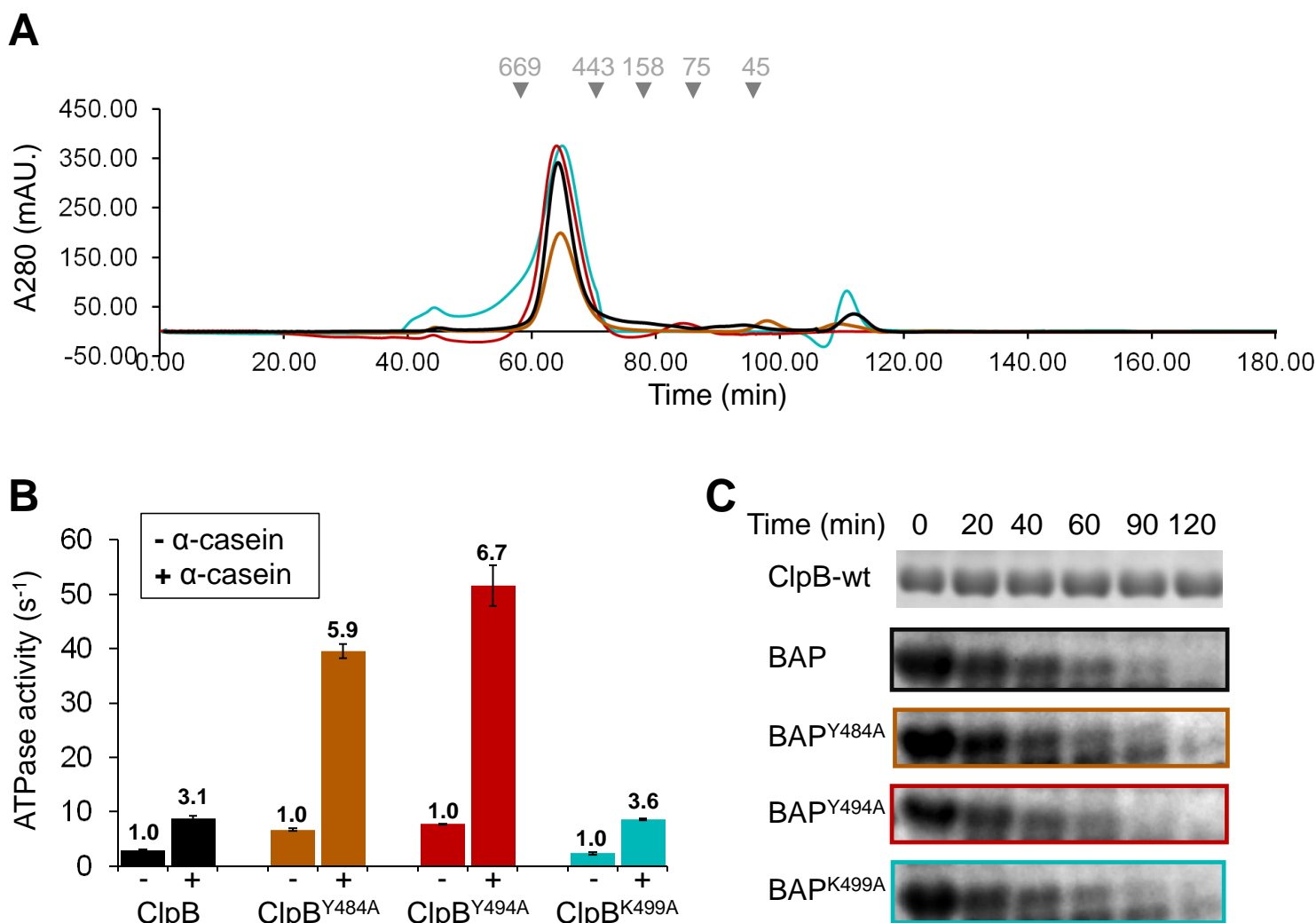


Fig. S7 ClpB Y484A, Y494A and K499A mutants display wt hexamerization and threading/translocation properties.

(A) Gel filtration analyses. The oligomerization state of ClpB (black), ClpB Y484A (orange), ClpB Y494A (red) and ClpB K499A (cyan) mutants in the presence of 1 mM ATP was analyzed by gel filtration (see “Materials and methods”). Arrowheads (▼) indicate the position of the sedimentation peak of thyroglobulin (669 kDa), apoferritin (443 kDa), aldolase (158 kDa), conalbumin (75 kDa) and ovalbumin (45 kDa). The elution profiles of all the ClpB mutants are indistinguishable from the wt hexameric ClpB protein. (B) ATPase activities of wt-ClpB or ClpB mutants were measured at 55 °C, in the absence or the presence of 0.1 mg/ml of α -casein. The ClpB K499A mutant demonstrated wt-ClpB ATP turnover rates, while ClpB Y494A and Y484A variants exhibit an increased basal ATPase activity and were hyperstimulated by α -casein as previously published (31). (C) Threading activities of ClpB mutants. α -Casein was incubated with ClpP and ClpB, TBAP or TBAP mutants, in the presence of 3 mM ATP at 55 °C. After 0, 20, 40, 60, 90 or 120 min incubation, the proteins were analyzed with SDS/PAGE, and the bands of α -casein are shown. Y484A (orange), Y494A (red) and K499A (cyan) ClpB mutants were as efficient as wt-BAP (black) in casein translocation and subsequent ClpP-dependent degradation.

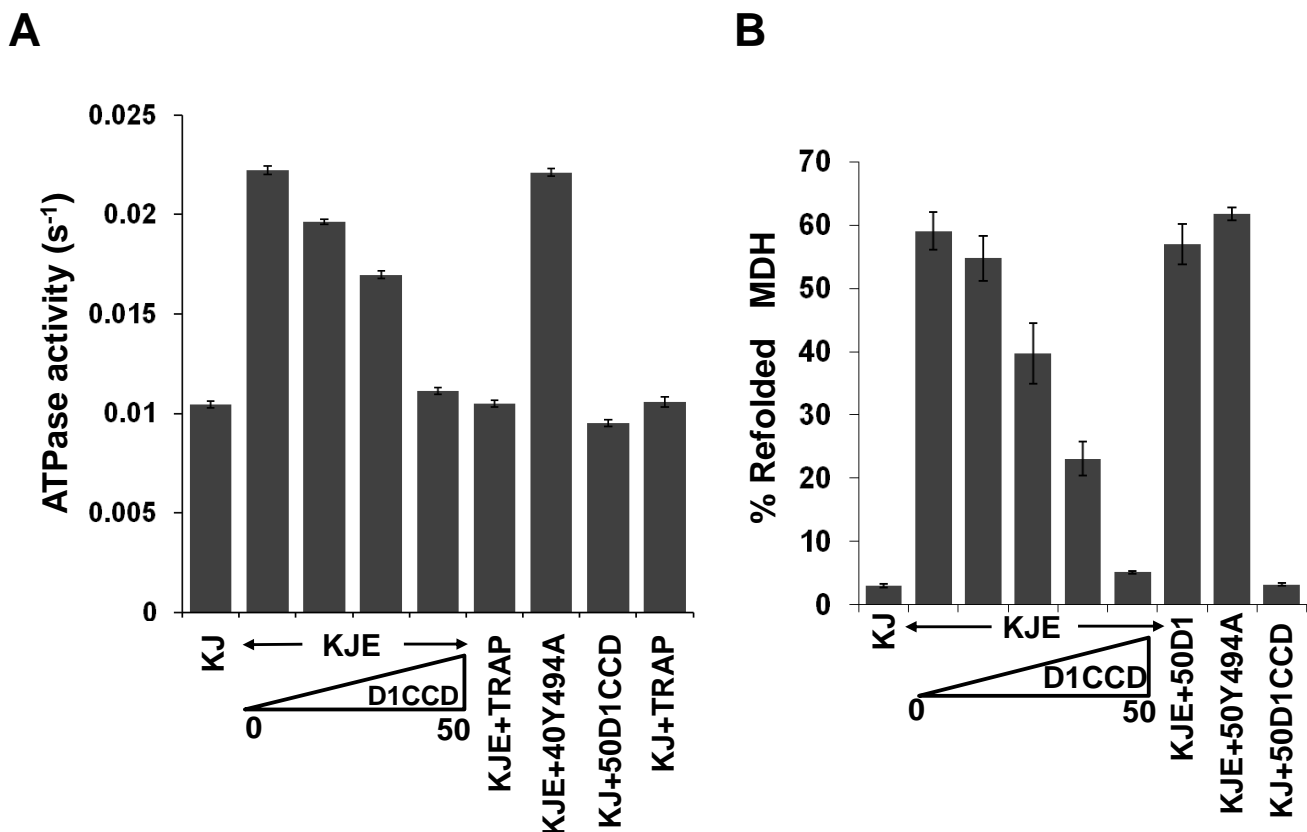


Fig. S8 ClpB^{NBD1-CCD} interaction with DnaK inhibits ATP hydrolysis rates and refolding functions of DnaK chaperone.

(A) Effect of ClpB^{NBD1-CCD} K204T mutant (D1CCD) or ClpB^{E271A/E268A} (TRAP) mutant on the ATPase activity of DnaK. The DnaJ-stimulated DnaK activity was measured either with (0.5 μM), or without GrpE in the presence of increasing concentrations (0, 5, 10, 20, 40 μM) of the ClpB^{NBD1-CCD} K204T mutant, that does not bind nucleotide, or the ClpB TRAP mutant, which binds but does not hydrolyze ATP. DnaK ATP turnover rates were quantified by measuring the release of inorganic phosphate (Pi). Data are presented as mean ± STD (*N* = 3). Addition of ClpB^{NBD1-CCD} K204T to DnaK/DnaJ/GrpE chaperones inhibited ATP hydrolysis rates of DnaK in a dose-dependent manner, while addition of ClpB^{NBD1-CCD} K204T to DnaK/DnaJ had no effect. The ClpB TRAP mutant inhibited DnaK ATPase turnover rates similarly to ClpB^{NBD1-CCD} K204T. ClpB^{NBD1-CCD} K204T/Y494A (labeled Y494A), which is incapable of interacting with DnaK, was used as a negative control and did not influence DnaK ATP turnover rates. (B) Percent of heat-denatured malate dehydrogenase (MDH) refolded by the DnaK/DnaJ/GrpE chaperone system in the presence of increasing concentrations (0, 5, 10, 20, 50 μM) of ClpB^{NBD1-CCD} K204T (D1CCD). MDH activity was measured after 120 min. Addition of ClpB^{NBD1-CCD} reduced the yield of reactivated MDH in a dose-dependent manner with complete inhibition at a 50:1 ClpB^{NBD1-CCD}: GrpE ratio. In control reactions, refolding was not appreciably inhibited by either ClpB^{NBD1}, which lacks the CCD (D1), or ClpB^{NBD1-CCD} with the Y494A substitution (labeled Y494A), which abrogates the ClpB/DnaK interaction.

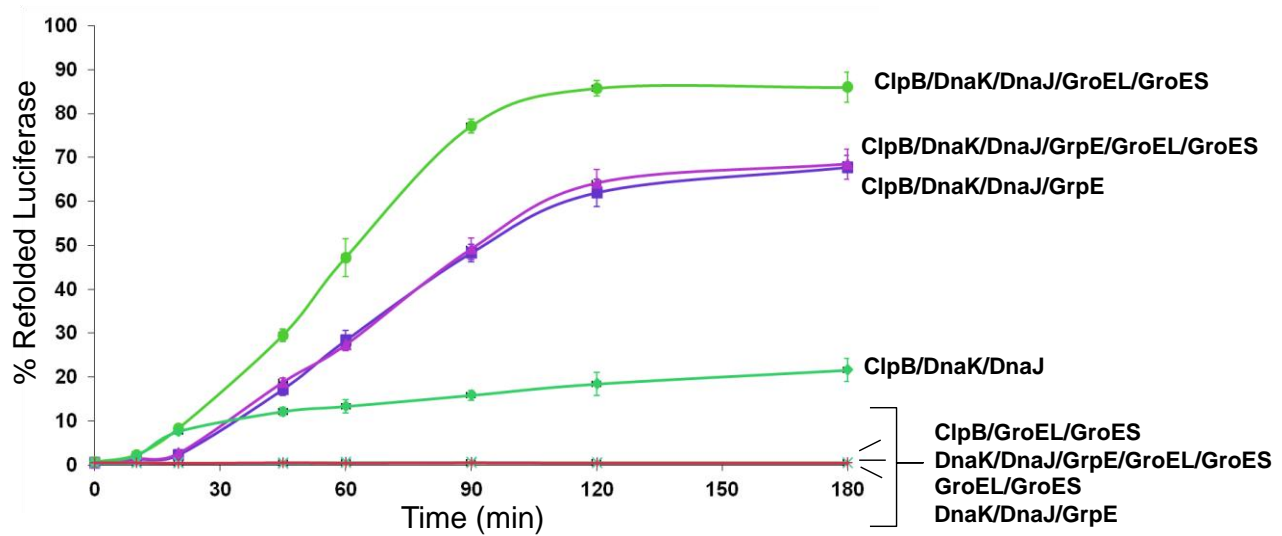


Fig. S9 GrpE is required only for the refolding of ClpB-unfolded substrates.

Reactivation of chemically-denatured luciferase was monitored in the presence of the ClpB/DnaK system with or without GrpE. Luciferase reactivation yields were measured over the course of 3 hours. In the presence of GrpE ~70% reactivation was observed while the addition of the GroEL/ES refolding chaperones to the reaction led to no further enhancement (compare blue and purple curves). Only ~20% reactivation of aggregated luciferase was possible in the presence of DnaK/DnaJ/ClpB, without the GrpE co-chaperone. However, once the GroEL/ES chaperone system was included in the reaction (no GrpE), faster rates and ~90% reactivation yields were observed. Thus, GrpE is not required in the initial steps of the disaggregation reaction, but functions downstream, together with DnaK/DnaJ, in refolding substrates, once these emerge from the ClpB central pore.

Table S1.**Apparent dissociation constants for DnaK and ClpB variants**

Protein	Protein labeling	Ligand	K_d (μM)	Nucleotide
ClpB ^{ΔNBD2}	U-[² H], ILV-[¹³ CH ₃]	DnaK	24.9 \pm 3.4	ADP
ClpB ^{ΔNBD2}	U-[² H], ILV-[¹³ CH ₃]	DnaK ^{NBD}	19.0 \pm 4.6	ADP
ClpB ^{NBD1-CCD}	U-[² H], ILV-[¹³ CH ₃]	DnaK	21.2 \pm 3.0	-
DnaK	U-[² H], ILV-[¹³ CH ₃]	ClpB ^{ΔNBD2}	24.0 \pm 2.4	ADP
DnaK ^{NBD}	U-[² H], ILV-[¹³ CH ₃]	ClpB ^{ΔNBD2}	20 \pm 2.6	ADP
DnaK ^{NBD}	U-[² H, ¹⁵ N]	ClpB ^{NBD1-CCD}	18.2 \pm 0.1	ADP
DnaK	U-[² H], ILV-[¹³ CH ₃]	ClpB ₆	26.6 \pm 4.2	ATP/ADP

^a All titration experiments were performed with fully deuterated unlabeled U-[²H, ¹²C, ¹⁴N] ligands. Listed dissociation constants are averages over values obtained from fitting titrations on a per-residue basis (typically 9-16 residues).

Table S2.

List of restraints used in the docking procedure

ClpB			
Active residues	L486, L490, L490, L492		
Passive residues	D482, Q483, Y484, N487, Y494, K499		
Flexible segments	G167-R175; G218-K227; E315-P326; L511-T522		
Fully flexible segments	E134-Y150		
DnaK			
Active residues	K54, R55, V58, L59, K248, Q249, E256, F277, A283, S284, K285		
Passive residues	G45, E46, R51, N230, E234, K238, E239		
Flexible segments	E28-L49; V58-E67; H240-D247; P276-H289		
PREs	Unambiguous Distance Restrains (Å) ^a	PREs	Unambiguous Distance Restrains (Å) ^a

ClpB			
^B 502SG – ^K 280δ1	14.0	^B 479SG – ^K 39γ1	21.0
^B 502SG – ^K 280δ2	14.2	^B 479SG – ^K 39γ2	19.7
^B 502SG – ^K 288δ1	18.7	^B 479SG – ^K 40γ1	23.2
^B 502SG – ^K 288δ1	20.9	^B 479SG – ^K 40γ2	24.1
^B 502SG – ^K 275δ1	23.2	^B 479SG – ^K 48δ1	14.1
^B 502SG – ^K 275δ2	22.3	^B 479SG – ^K 48δ2	14.4
^B 502SG – ^K 254δ1	20.8	^B 479SG – ^K 280δ1	22.6
^B 502SG – ^K 254δ2	21.0	^B 479SG – ^K 280δ2	22.9
^B 479SG – ^K 59δ1	14.0	^B 479SG – ^K 52ε	14.8
^B 479SG – ^K 59δ2	14.3	^B 77SG – ^K 39γ1	22.6
^B 479SG – ^K 58γ1	16.3	^B 77SG – ^K 40γ2	20.0
^B 479SG – ^K 49γ1	25.1	^B 77SG – ^K 115ε	20.0
^B 479SG – ^K 49γ2	25.1	^B 77SG – ^K 59δ1	21.2
^B 479SG – ^K 275δ1	23.1	^B 77SG – ^K 59δ2	23.0
^B 479SG – ^K 275δ2	22.7		

^a To get lower(upper) bounds subtract(add) 6Å(3Å), with the exception of residues with I_{ox}/I_{red}=0, where 10Å was used in place of 6Å.

Table S3.

Docking and structural statistics for the 95 best ClpB-DnaK model structures

	Ensemble	Representative structure
Docking statistics		
HADDOCK score	−45.4±2.8	−50
E _{vdw} [kcal/mol]	−38±3	−45
E _{elec} [kcal/mol]	−297±31	−302
E _{inter} [kcal/mol]	−228±33	−231
E _{AIR} [kcal/mol]	100±4	100.2
BSA [Å ²]	1402±36	1445
RMSD from lowest energy structure [Å]	0.41±0.21	0.2
Cluster size	95	-
Number of AIR violations > 0.3 Å	2±0	2

	Ensemble	Representative structure
Number of NOE violations > 0.3 Å	0	0
Structural statistics		
	0.56±0.1	
RMSD backbone (heavy atom) [Å]	(0.78±0.08)	-
RMSD all atoms at interface [Å]	0.89±0.1	-
RMSD backbone (heavy atom) from free ClpB [Å]	0.087±0.04 (0.88±0.04)	0.86 (0.86)
RMSD backbone (heavy atom) from free DnaK [Å]	0.67±0.08 (0.68±0.06)	0.66 (0.68)
Deviations from idealized geometry		
RMS deviation for bond angles [°]	0.6	0.6
RMS deviation for bond lengths [Å]	0.003	0.003
Ramachandran analysis, residues in		
Most favored regions [%]	88.4	88.6
Additionally allowed regions [%]	10.6	10.1
Generously allowed regions [%]	0.4	0.6
Disallowed regions [%]	0.6	0.8

References and Notes

1. D. A. Parsell, A. S. Kowal, M. A. Singer, S. Lindquist, Protein disaggregation mediated by heat-shock protein Hsp104. *Nature* **372**, 475 (Dec 1, 1994).
2. Y. Sanchez, S. L. Lindquist, HSP104 required for induced thermotolerance. *Science* **248**, 1112 (Jun 1, 1990).
3. J. Weibezahn *et al.*, Thermotolerance requires refolding of aggregated proteins by substrate translocation through the central pore of ClpB. *Cell* **119**, 653 (Nov 24, 2004).
4. J. R. Glover, S. Lindquist, Hsp104, Hsp70, and Hsp40: a novel chaperone system that rescues previously aggregated proteins. *Cell* **94**, 73 (Jul 10, 1998).
5. P. Goloubinoff, A. Mogk, A. P. Zvi, T. Tomoyasu, B. Bukau, Sequential mechanism of solubilization and refolding of stable protein aggregates by a bichaperone network. *Proc Natl Acad Sci U S A* **96**, 13732 (Nov 23, 1999).
6. A. Mogk *et al.*, Identification of thermolabile Escherichia coli proteins: prevention and reversion of aggregation by DnaK and ClpB. *EMBO J* **18**, 6934 (Dec 15, 1999).
7. K. Motohashi, Y. Watanabe, M. Yohda, M. Yoshida, Heat-inactivated proteins are rescued by the DnaK.J-GrpE set and ClpB chaperones. *Proc Natl Acad Sci U S A* **96**, 7184 (Jun 22, 1999).
8. M. P. Mayer, B. Bukau, Hsp70 chaperones: cellular functions and molecular mechanism. *Cell Mol Life Sci* **62**, 670 (Mar, 2005).
9. V. Tugarinov, P. M. Hwang, J. E. Ollerenshaw, L. E. Kay, Cross-correlated relaxation enhanced ^1H [bond] ^{13}C NMR spectroscopy of methyl groups in very high molecular weight proteins and protein complexes. *J Am Chem Soc* **125**, 10420 (Aug 27, 2003).
10. V. Tugarinov, L. E. Kay, An isotope labeling strategy for methyl TROSY spectroscopy. *J Biomol NMR* **28**, 165 (Feb, 2004).
11. R. Sprangers, L. E. Kay, Quantitative dynamics and binding studies of the 20S proteasome by NMR. *Nature* **445**, 618 (Feb 8, 2007).
12. I. Gelis *et al.*, Structural basis for signal-sequence recognition by the translocase motor SecA as determined by NMR. *Cell* **131**, 756 (Nov 16, 2007).
13. M. Miot *et al.*, Species-specific collaboration of heat shock proteins (Hsp) 70 and 100 in thermotolerance and protein disaggregation. *Proc Natl Acad Sci U S A* **108**, 6915 (Apr 26).
14. F. Seyffer *et al.*, Hsp70 proteins bind Hsp100 regulatory M domains to activate AAA+ disaggregase at aggregate surfaces. *Nat Struct Mol Biol* **19**, 1347 (Dec).
15. K. M. Flaherty, C. DeLuca-Flaherty, D. B. McKay, Three-dimensional structure of the ATPase fragment of a 70K heat-shock cognate protein. *Nature* **346**, 623 (Aug 16, 1990).
16. M. Sriram, J. Osipiuk, B. Freeman, R. Morimoto, A. Joachimiak, Human Hsp70 molecular chaperone binds two calcium ions within the ATPase domain. *Structure* **5**, 403 (Mar 15, 1997).
17. A. Zhuravleva, E. M. Clerico, L. M. Gierasch, An Interdomain Energetic Tug-of-War Creates the Allosterically Active State in Hsp70 Molecular Chaperones. *Cell* **151**, 1296 (Dec 7).

18. R. Kityk, J. Kopp, I. Sinning, M. P. Mayer, Structure and Dynamics of the ATP-Bound Open Conformation of Hsp70 Chaperones. *Mol Cell* **48**, 863 (Dec 28).
19. See supplementary materials on Science Online.
20. J. L. Battiste, G. Wagner, Utilization of site-directed spin labeling and high-resolution heteronuclear nuclear magnetic resonance for global fold determination of large proteins with limited nuclear overhauser effect data. *Biochemistry* **39**, 5355 (May 9, 2000).
21. T. L. Religa, R. Sprangers, L. E. Kay, Dynamic regulation of archaeal proteasome gate opening as studied by TROSY NMR. *Science* **328**, 98 (Apr 2).
22. C. Dominguez, R. Boelens, A. M. Bonvin, HADDOCK: a protein-protein docking approach based on biochemical or biophysical information. *J Am Chem Soc* **125**, 1731 (Feb 19, 2003).
23. S. J. de Vries *et al.*, HADDOCK versus HADDOCK: new features and performance of HADDOCK2.0 on the CAPRI targets. *Proteins* **69**, 726 (Dec 1, 2007).
24. C. J. Harrison, M. Hayer-Hartl, M. Di Liberto, F. Hartl, J. Kuriyan, Crystal structure of the nucleotide exchange factor GrpE bound to the ATPase domain of the molecular chaperone DnaK. *Science* **276**, 431 (Apr 18, 1997).
25. Y. Groemping *et al.*, Regulation of ATPase and chaperone cycle of DnaK from *Thermus thermophilus* by the nucleotide exchange factor GrpE. *J Mol Biol* **305**, 1173 (Feb 2, 2001).
26. C. Schlieker, I. Tews, B. Bukau, A. Mogk, Solubilization of aggregated proteins by ClpB/DnaK relies on the continuous extraction of unfolded polypeptides. *FEBS Lett* **578**, 351 (Dec 17, 2004).
27. J. P. Grimshaw, I. Jelesarov, H. J. Schonfeld, P. Christen, Reversible thermal transition in GrpE, the nucleotide exchange factor of the DnaK heat-shock system. *J Biol Chem* **276**, 6098 (Mar 2, 2001).
28. Y. Groemping, J. Reinstein, Folding properties of the nucleotide exchange factor GrpE from *Thermus thermophilus*: GrpE is a thermosensor that mediates heat shock response. *J Mol Biol* **314**, 167 (Nov 16, 2001).
29. T. Haslberger *et al.*, Protein disaggregation by the AAA+ chaperone ClpB involves partial threading of looped polypeptide segments. *Nat Struct Mol Biol* **15**, 641 (Jun, 2008).
30. S. Lee *et al.*, The structure of ClpB: a molecular chaperone that rescues proteins from an aggregated state. *Cell* **115**, 229 (Oct 17, 2003).
31. T. Haslberger *et al.*, M domains couple the ClpB threading motor with the DnaK chaperone activity. *Mol Cell* **25**, 247 (Jan 26, 2007).
32. P. Beinker, S. Schlee, R. Auvula, J. Reinstein, Biochemical coupling of the two nucleotide binding domains of ClpB: covalent linkage is not a prerequisite for chaperone activity. *J Biol Chem* **280**, 37965 (Nov 11, 2005).
33. T. Unger, Y. Jacobovitch, A. Dantes, R. Bernheim, Y. Peleg, Applications of the Restriction Free (RF) cloning procedure for molecular manipulations and protein expression. *J Struct Biol* **172**, 34 (Oct).
34. F. van den Ent, J. Lowe, RF cloning: a restriction-free method for inserting target genes into plasmids. *J Biochem Biophys Methods* **67**, 67 (Apr 30, 2006).

35. V. Tugarinov, V. Kanelis, L. E. Kay, Isotope labeling strategies for the study of high-molecular-weight proteins by solution NMR spectroscopy. *Nat Protoc* **1**, 749 (2006).
36. M. Revington, E. R. Zuiderweg, TROSY-driven NMR backbone assignments of the 381-residue nucleotide-binding domain of the *Thermus Thermophilus* DnaK molecular chaperone. *J Biomol NMR* **30**, 113 (Sep, 2004).
37. D. Klostermeier, R. Seidel, J. Reinstein, The functional cycle and regulation of the *Thermus thermophilus* DnaK chaperone system. *J Mol Biol* **287**, 511 (Apr 2, 1999).
38. D. Klostermeier, R. Seidel, J. Reinstein, Functional properties of the molecular chaperone DnaK from *Thermus thermophilus*. *J Mol Biol* **279**, 841 (Jun 19, 1998).
39. K. Amada *et al.*, Molecular cloning, expression, and characterization of chaperonin-60 and chaperonin-10 from a thermophilic bacterium, *Thermus thermophilus* HB8. *J Biochem* **118**, 347 (Aug, 1995).
40. R. Lum, M. Niggemann, J. R. Glover, Peptide and protein binding in the axial channel of Hsp104. Insights into the mechanism of protein unfolding. *J Biol Chem* **283**, 30139 (Oct 31, 2008).
41. T. L. Religa, A. M. Ruschak, R. Rosenzweig, L. E. Kay, Site-directed methyl group labeling as an NMR probe of structure and dynamics in supramolecular protein systems: applications to the proteasome and to the ClpP protease. *J Am Chem Soc* **133**, 9063 (Jun 15).
42. A. Guterman, M. H. Glickman, Complementary roles for Rpn11 and Ubp6 in deubiquitination and proteolysis by the proteasome. *J Biol Chem* **279**, 1729 (Jan 16, 2004).
43. F. Delaglio *et al.*, NMRPipe: a multidimensional spectral processing system based on UNIX pipes. *J Biomol NMR* **6**, 277 (Nov, 1995).
44. T. D. G. a. D. G. Kneller, *SPARKY 3*. (University of California, San Francisco).
45. K. L. Constantine *et al.*, Aliphatic ¹H and ¹³C resonance assignments for the 26-10 antibody VL domain derived from heteronuclear multidimensional NMR spectroscopy. *J Biomol NMR* **3**, 41 (Jan, 1993).
46. N. A. Farrow *et al.*, Backbone dynamics of a free and phosphopeptide-complexed Src homology 2 domain studied by ¹⁵N NMR relaxation. *Biochemistry* **33**, 5984 (May 17, 1994).
47. B. A. Lyons, M. Tashiro, L. Cedergren, B. Nilsson, G. T. Montelione, An improved strategy for determining resonance assignments for isotopically enriched proteins and its application to an engineered domain of staphylococcal protein A. *Biochemistry* **32**, 7839 (Aug 10, 1993).
48. T. M. Logan, E. T. Olejniczak, R. X. Xu, S. W. Fesik, A general method for assigning NMR spectra of denatured proteins using 3D HC(CO)NH-TOCSY triple resonance experiments. *J Biomol NMR* **3**, 225 (Mar, 1993).
49. G. M. Clore, A. Bax, P. C. Driscoll, P. T. Wingfield, A. M. Gronenborn, Assignment of the side-chain ¹H and ¹³C resonances of interleukin-1 beta using double- and triple-resonance heteronuclear three-dimensional NMR spectroscopy. *Biochemistry* **29**, 8172 (Sep 4, 1990).

50. C. Zwahlen, S. J. F. Vincent, K. H. Gardner, L. E. Kay, Significantly improved resolution for NOE correlations from valine and isoleucine (C-gamma 2) methyl groups in N-15,C-13- and N-15,C-13,H-2-labeled proteins. *Journal of the American Chemical Society* **120**, 4825 (May 20, 1998).
51. K. Pervushin, R. Riek, G. Wider, K. Wuthrich, Attenuated T-2 relaxation by mutual cancellation of dipole-dipole coupling and chemical shift anisotropy indicates an avenue to NMR structures of very large biological macromolecules in solution. *Proceedings of the National Academy of Sciences of the United States of America* **94**, 12366 (Nov 11, 1997).
52. M. Salzmann, K. Pervushin, G. Wider, H. Senn, K. Wuthrich, TROSY in triple-resonance experiments: new perspectives for sequential NMR assignment of large proteins. *Proc Natl Acad Sci U S A* **95**, 13585 (Nov 10, 1998).
53. M. Salzmann, G. Wider, K. Pervushin, H. Senn, K. Wuthrich, TROSY-type triple-resonance experiments for sequential NMR assignments of large proteins. *J Am Chem Soc* **121**, 844 (Nov 25, 1999).
54. V. Tugarinov, W. Y. Choy, V. Y. Orekhov, L. E. Kay, Solution NMR-derived global fold of a monomeric 82-kDa enzyme. *Proc Natl Acad Sci U S A* **102**, 622 (Jan 18, 2005).
55. D. Neri, T. Szyperski, G. Otting, H. Senn, K. Wuthrich, Stereospecific nuclear magnetic resonance assignments of the methyl groups of valine and leucine in the DNA-binding domain of the 434 repressor by biosynthetically directed fractional ¹³C labeling. *Biochemistry* **28**, 7510 (Sep 19, 1989).
56. N. Tjandra, H. Kuboniwa, H. Ren, A. Bax, Rotational dynamics of calcium-free calmodulin studied by ¹⁵N-NMR relaxation measurements. *Eur J Biochem* **230**, 1014 (Jun 15, 1995).
57. J. Garcia de la Torre, M. L. Huertas, B. Carrasco, HYDRONMR: prediction of NMR relaxation of globular proteins from atomic-level structures and hydrodynamic calculations. *J Magn Reson* **147**, 138 (Nov, 2000).
58. V. Tugarinov, L. E. Kay, Relaxation rates of degenerate ¹H transitions in methyl groups of proteins as reporters of side-chain dynamics. *J Am Chem Soc* **128**, 7299 (Jun 7, 2006).
59. S. A. T. W. H. Press, W. T. Vetterling, B. P. Flannery, *Numerical Recipes in C. The Art of Scientific Computing*. Cambridge University Press **Cambridge**, (1999).
60. S. J. a. T. Hubbard, J.M., *NACCESS*. (Department of Biochemistry and Molecular Biology, University College London, 1993).
61. A. B. Biter, S. Lee, N. Sung, F. T. Tsai, Structural basis for intersubunit signaling in a protein disaggregating machine. *Proc Natl Acad Sci U S A* **109**, 12515 (Jul 31).
62. P. Beinker, S. Schlee, Y. Groemping, R. Seidel, J. Reinstein, The N terminus of ClpB from *Thermus thermophilus* is not essential for the chaperone activity. *J Biol Chem* **277**, 47160 (Dec 6, 2002).
63. S. Diamant, A. Azem, C. Weiss, P. Goloubinoff, Increased efficiency of GroE-assisted protein folding by manganese ions. *J Biol Chem* **270**, 28387 (Nov 24, 1995).
64. I. Wolfram Research. (Champaign, IL, 2010).

65. J. G. Norby, Coupled assay of Na⁺,K⁺-ATPase activity. *Methods Enzymol* **156**, 116 (1988).
66. D. L. Stiggall, Y. M. Galante, Y. Hatefi, Preparation and properties of complex V. *Methods Enzymol* **55**, 308 (1979).
67. E. Shacter, Organic extraction of Pi with isobutanol/toluene. *Anal Biochem* **138**, 416 (May 1, 1984).